Chalcogenide Letters Vol. 20, No. 12, December 2023, p. 871 - 882

Effect of the back contact electrode on the performances of the ultra-thin photovoltaic cells based on the CdS/CdTe heterojunction

A.M. Raduta[a,b], A.M. Panaitescu[a], A. Radu[a], L. Ion[a], V.A. Antohe[a,c], O. Toma[a], S. Iftimie[a], S. Antohe[a,d,*]

[a]*University of |Bucharest, Faculty of Physics, R&D Center for Materials and Electronic & Optoelectronic Devices (MDEO), 405 Atomistilor Street, PO Box MG-11, Bucharest-Magurele, 077125, Romania*

[b]*The National Institute for Research and Development for Optoelectronics- INOE 2000, 409 Atomistilor Street, 077125, Magurele, Romania*

[c]*Université Catholique de Louvain (UCLouvain), Institute of Condensed Matter and Nanosciences (IMCN), Place Croix du Sud 1, B-1348 Louvain-la-Neuve, Belgium*

[d]*Academy of Romanian Scietists, Ilfov Street 3, 050045 Bucharest, Romania*

This paper proposes a comparative study between two sub-micrometric multi-layered photovoltaic cells, based on A_{II}–B_{VI} compounds, using different structures for the holes transport and collection electrode. Using the modified form of the Shockley equation, the diode factor, n, the reverse saturation current, I_0, and the series R_s and shunt R_{sh} resistances were evaluated and their effect on the photovoltaic cells performances were discussed. The photovoltaic performances were analysed by current-voltage characteristics at illumination in standard AM 1.5 conditions, and the specific parameters were determined.

(Received October 6, 2023; Accepted December 5, 2023)

Keywords: CdS/CdTe heterojunction, Photovoltaic devices, Modified Shockely equation, Ultra-thin films

1. Introduction

A photovoltaic device based on cadmium telluride (CdTe) as the main absorber and cadmium sulphide (CdS) as a window layer in the heterojunction (CdS/CdTe) can be considered a classical one. Still, despite this, the optimization process is far from being ended, and one of the aspects which are continuously enhanced is the power conversion efficiency (PCE). In this sense, in 2001, PCE was around 17% for individual structures [1] and it overpassed 21% in 2020 [2], while for large area modules, the reported record value was around 19% [2]. Such performance indicates alike devices are suitable candidates to operate together with silicon-based technology configurations.

Because CdS/CdTe heterojunction has the benefit of an almost ideal energy band alignment and a very good match of their crystalline structures, both space and terrestrial applications were developed. After D.L. Batzner [3] et al. opened the door for CdS/CdTe heterojunction-based solar cells for space applications, many research groups improved both the devices' stability and performances. S. Antohe et al. demonstrated irradiation with alpha particles of energy of 3 MeV and 10^{13} $parcticles/cm^2$ fluency leads to an increase of point-like defects at the CdS/CdTe interface [4], but in the same times, they showed that the stability against protons of energy of 3 MeV an 10^{14} $particles/cm^2$ fluency can be improved by modifying the transparent electrode [5]. Nevertheless, the majority of applications as photovoltaic devices are built for terrestrial usage, but due to relatively high stability at ionizing radiation, they are used in space applications too, operating in relatively high background of cosmic rays. The large values of both CdS and CdTe's absorption coefficients [6] together with their direct energy bands alignment; i.e.

* Corresponding author: santohe@solid.fizica.unibuc.ro
https://doi.org/10.15251/CL.2023.2012.871

$2.3 - 2.4$ eV for CdS [7] and $1.43 - 1.45$ eV for CdTe [8], for bulk materials and with small variations for confined structures, increased and varied the assigned applications. Versatility in terms of easy building architectures is another attribute of CdS and CdTe materials, so the optimization of CdS/CdTe device performances may be performed by different approaches; i.e. E. Artegiani et al. analysed the influence of the transparent electrode on the photo-electrical response and time stability for a superstrate structure by testing an indium tin oxide/zinc oxide (ITO/ZnO) configuration compared to individual ITO and/or fluorine tin oxide (FTO) [9], while X. Mathew et al. took a step forward and fabricated CdS/CdTe devices onto flexible substrates [10]. The use of different substrates was possible because both CdS and CdTe thin films can grow by assorted methods, including thermal evaporation [8, 11-13], radio-frequency (RF) magnetron sputtering [8, 14-16], close-space sublimation [17,18], electrodeposition [8,19,20], and molecular beam epitaxy [21,22]. Despite so many obtaining alternatives, the literature reports indicate thermal evaporation as the main approach and due to this, the thickness of samples is usually about $2 - 3$ μm. In this work, we have chosen RF magnetron sputtering as the main technique to grow CdS and CdTe ultra-thin films for photovoltaic devices because this method has the advantage of a good control of the film thickness [23,24]. Also, the use of a plasma-based deposition technique has the advantage of the employment of ions, so the purity control during the growth process is improved [24].

The goal of this paper is to report our results on the preparation of a substrate structure, Ag/ZnPc/ZnTe/CdTe/CdS/ZnO/ITO, using as back contact a multi-layered architecture, Ag/ZnPc/ZnTe, which also supports the holes transport and collection to electrode (HTCE) and to discuss its performance in terms of ITO_A/CdTe/CdS/ZnO/ITO, for which the HTCE is the glass substrate covered with ITO ($8 - 12\ \Omega/\mathrm{cm}^2$), commercially available. We made a solid comparison in terms of their electrical and photo-electrical parameters between the two CdS/CdTe thin film-based photovoltaic devices, having the same electron transport and collection electrode (ETCE), namely ZnO/ITO. Being a direct and wide bandgap semiconductor (2.26 eV), with low electron affinity (3.53 eV) and high electrical mobility, zinc telluride (ZnTe) is frequently used in the CdTe-based superstrate photovoltaic devices, especially as hole transport layer [25-28]. In order to avoid possible shortcuts that may appear during the fabrication of CdS and CdTe ultra-thin films, zinc phthalocyanine (ZnPc) was used. The transparent conductive oxide of all obtained photovoltaic devices contains ZnO as buffer layer to improve the electron collection to negative electrode. In this respect, we have evaluated and discussed the ideality diode factor (n), the reverse saturation current (I_0), the series (R_s) and shunt (R_{sh}) resistances, open circuit photo-voltage (V_{oc}), short-circuit current density (J_{sc}), maximum output power (P_{max}), and the fill factor (FF).

2. Experimental

The schematic representation and the energy band diagram of the Glass/Ag/ZnPc/ZnTe/CdTe/CdS/ZnO/ITO and Glass/ITO_A/CdTe/CdS/ITO built photovoltaic devices are shown in Figure 1. In this paper, the glass/ITO_A denotes indium tin oxide coated glass slides, commercially available from Merck Company, with a sheet resistance of $8 - 12\ \Omega/\mathrm{cm}^2$, and the ITO simple notation is used for the home-growth oxide film as part of the fabricated architectures, by RF magnetron sputtering.

For Glass/Ag/ZnPc/ZnTe/CdTe/CdS/ZnO/ITO device, except for the silver/zinc phthalocyanine (Ag/ZnPc) architecture, which was deposited by thermal evaporation, all the other component layers were obtained by RF magnetron sputtering; ZnTe, CdTe, CdS, and ZnO. The used magnetron sputtering equipment was a Tectra Company one (Germany), with capabilities of both radio-frequency (RF) and direct current (DC) deposition modes. The ZnTe, CdTe, and CdS targets were purchased from FHR Anlagenbau GmbH Company (Germany) and their geometrical features were 50.8 mm in diameter and 3 mm in thickness. The purity of targets was 99.99%. The ZnO sputtering target was bought from Neyco Company (France) and it is 50.8 mm in diameter and 3 mm in thickness; the purity was 99.95%. The ZnPc powder was acquired from Merck

Company (Germany); the CAS number was 14320-04-8, and the purity was 97%. Before starting any deposition process, the optical glass substrates were cleaned in ultra-sonic bath following the next procedure, i.e. 15 minutes in acetone, 15 minutes in isopropyl alcohol, and 15 minutes in pure water, type 3, obtained from a Direct-Q 3 UV Milipore water purification system. The drying process was done under nitrogen flow.

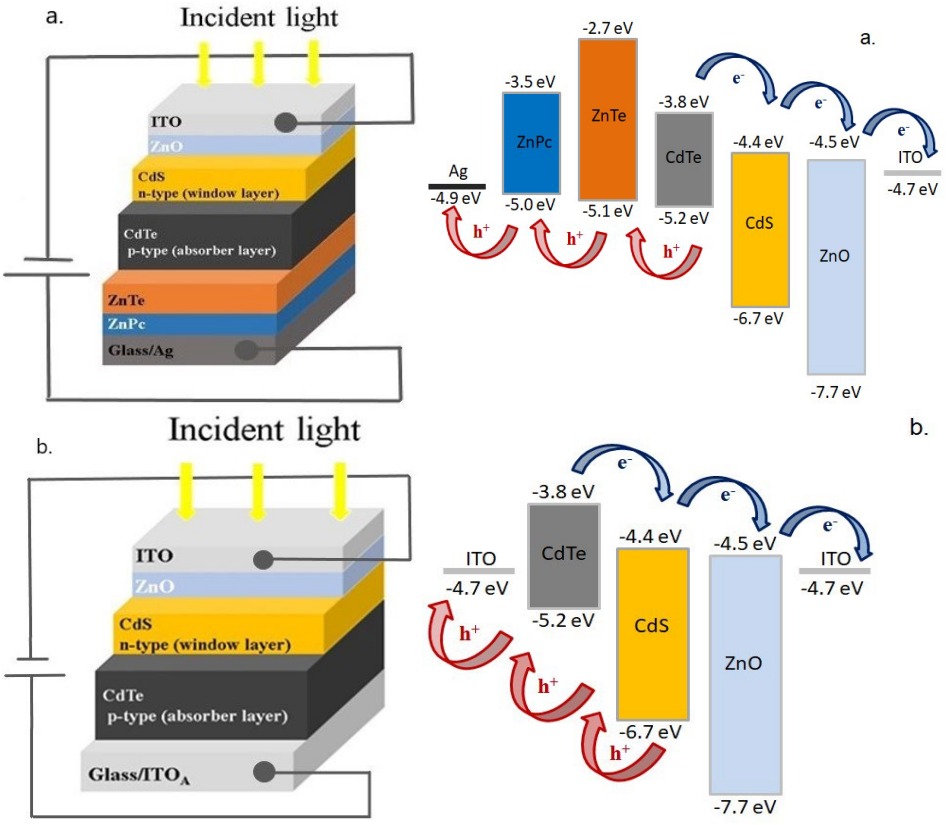

Fig. 1. Schematic representation and energy bandgap diagram of (a) Glass/Ag/ZnPc/ZnTe/CdTe/CdS/ZnO/ITO and (b) Glass/ITO$_A$/CdTe/CdS/ZnO/ITO photovoltaic devices.

The presence of the ZnO layer, deposited before the ITO, creates a neglected energy barrier for electrons but a high barrier for holes at the interface with CdS [29]. In this way, the electron collection is facilitated. On the other hand, for the Glass/Ag/ZnPc/ZnTe/CdTe/CdS/ZnO/ITO device we customized the p-part of the p-n heterojunction by growing two layers, namely ZnPc and ZnTe. The used values for electrodes' work function and inorganic materials' bandgap and their corresponding molecular orbitals assigned to organic materials were collected from literature, from studies discussing similar architectures; ITO and ZnO [29], Ag [25,26,30], CdS [31], CdTe [32], ZnTe [25,26,33], and ZnPc [34].

For the Glass/ITO$_A$/CdTe/CdS/ZnO/ITO, except for the ITO$_A$-coated commercially available glass substrates, all the layers were prepared by RF magnetron sputtering in the same conditions as the films used in Glass/Ag/ZnPc/ZnTe/CdTe/CdS/ZnO/ITO structures.

The deposition parameters, together with their evaluated thickness, of all component thin films of Glass/Ag/ZnPc/ZnTe/CdTe/CdS/ZnO/ITO and Glass/ITO$_A$/CdTe/CdS/ZnO/ITO prepared devices are displayed in Table 1. The thickness of the component layers was adapted considering other similar studies from the literature. Based on the results obtained in [35], we have increased the thickness of the ITO film, and, in order not to expand the thickness of the electron collection electrode too much, we considered the same thickness for the ZnO layer. The ZnTe thickness was

set up considering the study presented in [36], and a reference for the CdS film's thickness can be found in [7]. Because the back contact was tailored as a multi-layered architecture, namely Ag/ZnPc/ZnTe, and because the thickness of ZnTe and Ag layers were set on (the metallic contact was designed to have the same thickness as the transparent conductive electrode), in order not to grow up too much the series resistance of the whole device with the thickness, the ZnPc buffer film was considered to be half of the other two components of the HTCE. Usually, the thickness of the CdTe absorber layer for such devices is between $1-3$ μm but in this paper, we have discussed an ultra-thin CdS/CdTe heterojunction, so we have decided to strongly reduce its thickness, by considering to be about half of 1 μm. A related reference is [37]. Of course, the optimization process implies further studies, as it is suggested in [38, 39].

Table 1. The fabrication details of Ag, ZnPc, ZnTe, CdTe, CdS, and ITO ultra-thin films; for Glass/Ag/ZnPc/ZnTe/CdTe/CdS/ZnO/ITO and Glass/ITO$_A$/CdTe/CdS/ZnO/ITO built photovoltaic devices.

Ultra-thin film	Ag	ZnPc	ZnTe	CdTe	CdS	ZnO	ITO
Deposition method	TVE	TVE	RF magnetron	RF mag-netron	RF magnetron	RF magnetron	RF magnetron
Source temperature (℃)	1000	325	-	-	-	-	-
Substrate temperature (℃)	100	50	200	230	230	RT	RT
Working pressure (Pa)	4×10^{-3}	4×10^{-3}	2.5	8.6	8.6	6.3	8.6
Working power (W)	-	-	50	35	35	50	80
Deposition rate $(Å/sec)$	20	5	-	-	-	-	-
Deposition time (min)	1	2	10	60	20	45	30
Thickness (nm)	100 - QCM	60 - QCM	100 - QCM	563 - OT	51 - XRR	50 - QCM	100 - QCM

QCM – quartz crystal monitor; OT – optical transmission spectroscopy; XRR – X-ray reflectometry;

The electrical behaviour of fabricated photovoltaic devices was analysed by current-voltage (I-V) characteristics in dark; the main parameters such as series (R_s) and shunt (R_{sh}) resistances, the reverse saturation current (I_0), and the ideality factor (n) of a diode were determined and discussed. Moreover, to evaluate the performances as photo-element, the I-V characteristics at illumination in AM 1.5 conditions (incident power density equal to $100\,mW/cm^2$) were drawn and the typical parameters, the open circuit photo-voltage (V_{oc}), short-circuit current density (J_{sc}), maximum output power (P_{max}), and fill factor (FF) were calculated and compared. Optical glass substrates of 11mm width and 21 mm length was used, and the active area of fabricated photovoltaic devices was 0.40 cm^2 . The experimental set-up consisted of a Keithley Source Meter 2400 equipment and, for the I-V characteristics at illumination, a Newport Oriel solar simulator. All devices were controlled by the computer. The measurements were performed in the air, at room temperature.

3. Results and discussions

3.1. Electrical and photo-electrical results for Ag/ZnPc/ZnTe/CdTe/CdS/ZnO/ITO structures

As shown in Figure 2a, the dark voltage characteristics emphasize a nonlinear and asymmetrical behaviour, with a low value for the rectifying factor. In order to fit the forward characteristic most favourable and to evaluate the values of shunt and series resistances, an effective model based on the modified Shockley-Read equation was considered:

$$I = I_0\left\{e^{\left|\frac{q(V-IR_S)}{nk_BT}\right|} - 1\right\} + \frac{V-IR_S}{R_{sh}} \quad (1)$$

in which I_0 is the saturation current, n is the ideality diode factor, R_s is the series resistance, and R_{sh} is the shunt resistance of the structure.

The semilogarithmic plot of the dark I-V characteristics at forward bias is shown in Figure 2b. From the linear part of $ln(I_{dark})\ vs.V$ plot, the slope $\left(\beta = \frac{q}{nk_BT} = 12.06\right)$ was obtained, then resulting for the ideality diode factor the value $n = 3.19$. The intercept of the straight line with the current axis gave the value of $I_0 = 3.24 \times 10^{-8}A$ for the saturation current. Both values of n and I_0 obtained just from the fit described above (inserted in Figure 2b) are affected on a relatively short range of voltage $(0.13 - 0.28)\,V$. To increase the accuracy of the evaluation of these parameters, the effect of R_s and R_{sh} has to be removed.

The values of series and shunt resistances were determined from the analysis of the dependence of differential resistance R_0 on the reverse saturation current at forward bias, as can be seen in Figure 2c. According to euqation (1), the differential resistance is given by:

$$R_0 = \frac{dU}{dI} = R_s + \frac{1}{\beta I_0 e^{\beta(V-IR_S)} + \frac{1}{R_{sh}}} \quad (2)$$

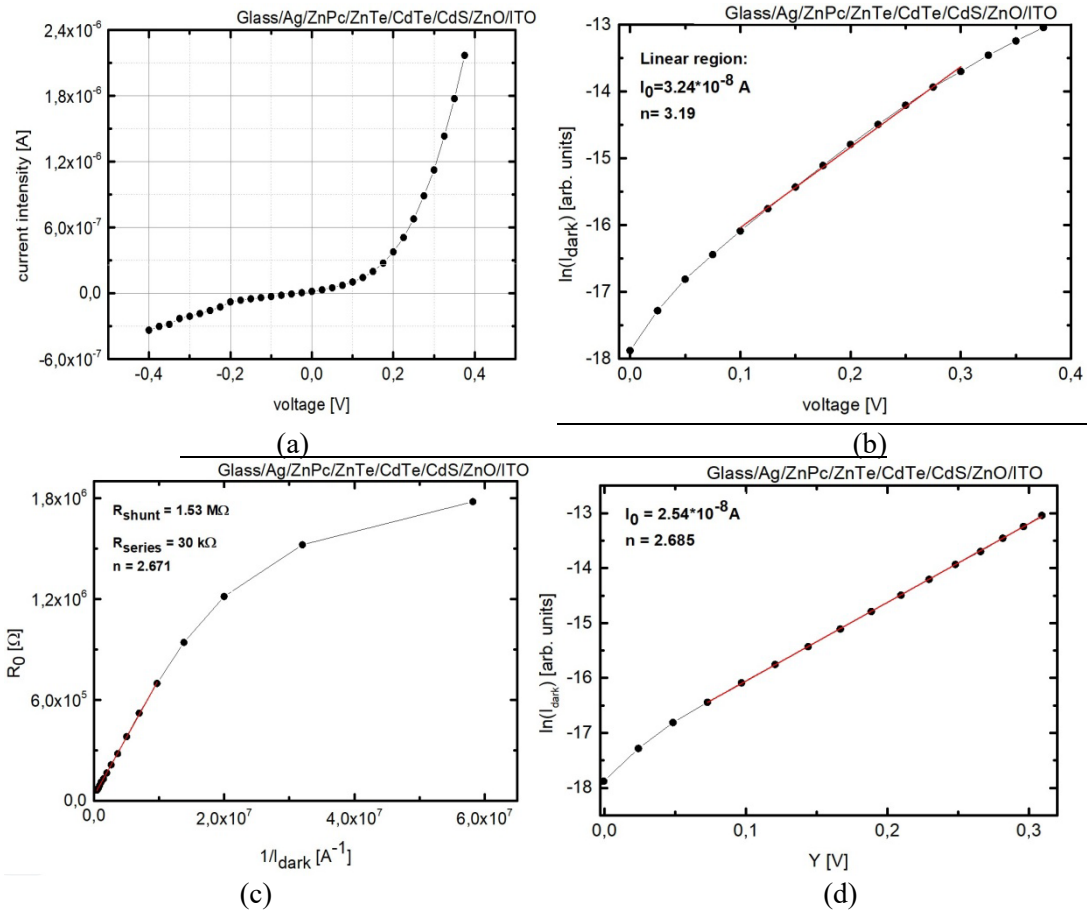

Fig. 2. (a) Current-voltage characteristics in dark for Glass/Ag/ZnPc/ZnTe/CdTe/CdS/ZnO/ITO photovoltaic structure;(b) The dark forward I-V characteristics of the glass/Ag/ZnPc/ZnTe/CdTe/CdS/ZnO/ITO photovoltaic structure in semilogarithmic plot; first evaluation for n – the ideality diode factor and I_0 – the reverse saturation current; (c) $R_0\ vs.\frac{1}{I_{dark}}$ plot corresponding to Glass/Ag/ZnPc/ZnTe/CdTe/CdS/ZnO/ITO photovoltaic structure; an evaluation for n, R_s, and R_{sh}; (d) $\ln(I_{dark})\ vs.Y$ dependence for Glass/Ag/ZnPc/ZnTe/CdTe/CdS/ZnO/ITO photovoltaic structure for the new variable $Y = V - IR_s$.

According to equation (2), the R_0 vs. $\frac{1}{I_{dark}}$ plot can be divided in two regions: the region of high currents and the region of low currents, respectively. From the first extrapolated linear region, the evaluated value of n from the slope was 2.671, while the intercept was exactly R_s, which in this case was 30 kΩ, and R_{sh} was 1.53 MΩ.

To improve the linearity of $ln(I)\ vs.V$ dependence and to determine the values of n and I_0 with higher accuracy, the effect of R_s was removed by making the following change in the variable: $Y = V - IR_s$. By using the new variable and considering Y the voltage only across the heterojunction [40, 41], the equation (1) becomes:

$$I = I_0\left[e^{\beta Y} - 1\right] + \frac{Y}{R_{sh}} \tag{3}$$

Thus, by plotting $ln(I)\ vs.Y$, another approximation for n and I_0 can be obtained, as is shown in Figure 2d.

By this new approximation, the linear region extends from 0.07 V to 0.3 V. By removing the effects induced by the series resistance, the obtained values for n and I_0 were 2.685 and 2.54×10^{-8}A, respectively. The final step to obtain highly accurate values for n and I_0 is the semilogarithmic plot of real current $I - \frac{Y}{R_{sh}}$ crossing the heterojunction as a function of Y, that obeys the modified Shockley-Read equation, denoted here as equation (3) (see Figure 3).

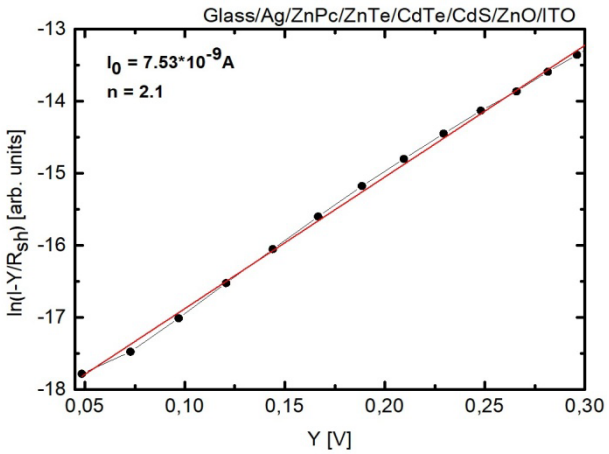

Fig. 3. Semilogarithmic plot $ln\left(I - \frac{Y}{R_{sh}}\right)\ vs.Y$ of the forward bias dark current of the Glass/Ag/ZnPc/ZnTe/CdTe/CdS/ZnO/ITO structure.

From the enlarged straight line in Figure 3, the values of n and I_0 were determined as 2.1 and 7.53×10^{-9} A, respectively. One can easily see that, after removing the effects of both series and shunt resistances, the linearity in the plot from Figure 3 was extended, allowing a better evaluation of parameters.

The relatively high values obtained for the ideality diode factor, ranging from 2.1 to 3.19, depending on the used approximation, is comparable to other similar structures and are typically expected for thin film-based devices due to the fine grain structure of the components.

The external quantum efficiency (EQE) of the prepared structures was measured at room temperature, in air, using an experimental set-up consisting of a Keithley Source Meter 2400 model, a Newport Oriel monochromator, and a Newport Oriel solar simulator. The action spectrum of Glass/Ag/ZnPc/ZnTe/CdTe/CdS/ZnO/ITO built device is shown in Figure 4.

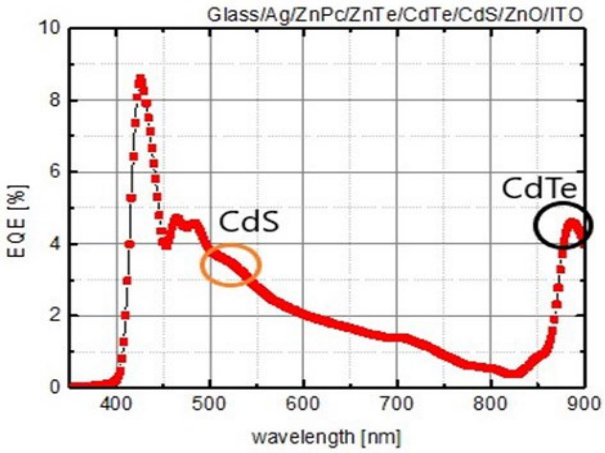

Fig. 4. The action spectrum of the fabricated Glass/Ag/ZnPc/ZnTe/CdTe/CdS/ZnO/ITO photovoltaic structure.

The maxima corresponding to the main contributors to photo-generation, CdTe as the absorber layer and CdS as the window layer were easily detected but the photovoltaic response due to the CdS/CdTe heterojunction is very low. The existence of a shoulder instead of an individual maximum around 540 nm may be related to the presence of the ZnTe thin film, which has an optical bandgap of 2.27 eV, suggesting its contribution to photo-generation too. Unfortunately, the photovoltaic response is reduced due to a poor collection of the photo-generated carriers; electrons at ZnO/ITO top electrode and holes at the Ag back contact electrode, respectively.

The current-voltage characteristics in AM 1.5 (see Figure 5) conditions confirm the behaviour indicated by the action spectra and revealed a series resistance, which lowered the fill factor and the overall power conversion efficiency. However, as a positive effect of the multi-layered configuration, we can indicate a high shunt resistance, too.

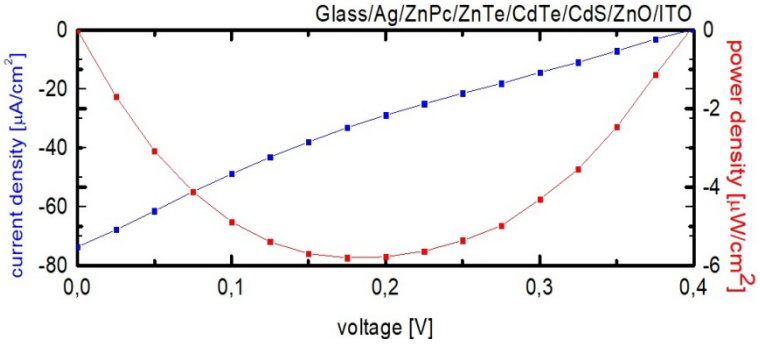

Fig. 5. The current density – voltage (blue line) and power density – voltage (red line) characteristics in AM 1.5 conditions for Glass/Ag/ZnPc/ZnTe/CdTe/CdS/ZnO/ITO photovoltaic device.

Table 2. The typical parameters in the photo-element regime for Glass/Ag/ZnPc/ZnTe/CdTe/CdS/ZnO/ITO photovoltaic device.

Sample	V_{oc} (mV)	J_{sc} $(\mu A/cm^2)$	P_{max} (μW)	FF (%)
Glass/Ag/ZnPc/ZnTe/CdTe/CdS/ZnO/ITO	400	73.6	5.8	20

3.2. Electrical and photo-electrical results for the Glass/ITO$_A$/CdTe/CdS/ZnO/ITO structures

For Glass/ITO$_A$/CdTe/CdS/ZnO/ITO photovoltaic structure, to evaluate the diode factor (n), the reverse saturation current (I_0), the series (R_s) and the shunt (R_{sh}) resistances, the same protocol as in the case of Glass/Ag/ZnPc/ZnTe/CdTe/CdS/ZnO/ITO samples was applied.

The current-voltage (I-V) characteristics in dark for both forward and reverse bias are presented in Figure 6.

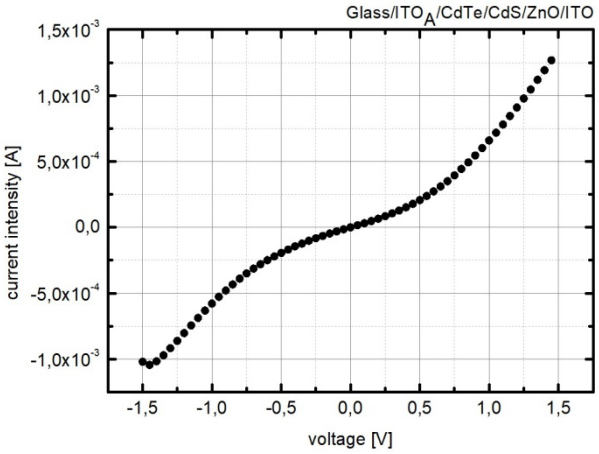

Fig. 6. I-V dark characteristic of the Glass/ITO$_A$/CdTe/CdS/ZnO/ITO structure recorded at room temperature – forward and reverse bias.

As one can easily observe, the very low asymmetry of the I-V characteristic suggests a small value of the shunt resistance of the cell but for a rigorous comparison with the previously described structure, using the modified Shockley-Read equation, the values of n, I_0, R_s, and R_{sh} were determined following the protocol described above. To better compare the typical electrical parameters for the obtained samples, Table 3 sums up the values for the evaluated electrical parameters.

Table 3. The values of the typical electrical parameters characterizing the Glass/Ag/ZnPc/ZnTe/CdTe/CdS/ZnO/ITO and Glass/ITO$_A$/CdTe/CdS/ZnO/ITO structures, obtained by the fit of experimental data with the modified form of the Shockley-Read equation. The plot f_1 is $ln(I) = f(U)$. The plot f_2 is $ln(I) = f(Y)$. The plot f_3 is $ln\left(I - \frac{Y}{R_{sh}}\right) = f(Y)$.

Sample	R_s $(k\Omega)$	R_{sh} $(M\Omega)$	I_0 (μA)	n
Glass/Ag/ZnPc/ZnTe/CdTe/CdS/ZnO/ITO	3	1.53	0.0324 - f_1	3.19 - f_1
			0.0254 - f_2	2.68 - f_2
			0.00753 - f_3	2.1 - f_3
Glass/ITO$_A$/CdTe/CdS/ZnO/ITO	0.48	0.003	3.23 - f_1	10.5 - f_1
			3.78 - f_2	9.58 - f_2
			0.7 - f_3	6.68 - f_3

One may observe that, as it was above comment, in the case of Glass/Ag/ZnPc/ZnTe/CdTe/CdS/ZnO/ITO photovoltaic device, due to an increased number of interfaces compared to Glass/ITO$_A$/CdTe/CdS/ZnO/ITO structure, both the series and shunt resistances are about one and three orders of degree higher, respectively. The ideality diode factor and the reverse saturation current have larger values for Glass/ITO$_A$/CdTe/CdS/ZnO/ITO samples,

in this way, explaining the poor asymmetry of the I-V characteristics. The electrical behaviour of this structure in dark is supported by its spectral response, shown in Figure 7.

The action spectra of Glass/ITO$_A$/CdTe/CdS/ZnO/ITO device clearly evidence the threshold wavelength for direct optical transitions for CdTe and CdS, and, overall, an increased value of the external quantum efficiency, evaluated for the visible range of solar spectrum.

The photo-electrical behaviour of Glass/ITO$_A$/CdTe/CdS/ZnO/ITO photovoltaic structure is presented in Figure 8, while the specific parameters are collected in Table 4.

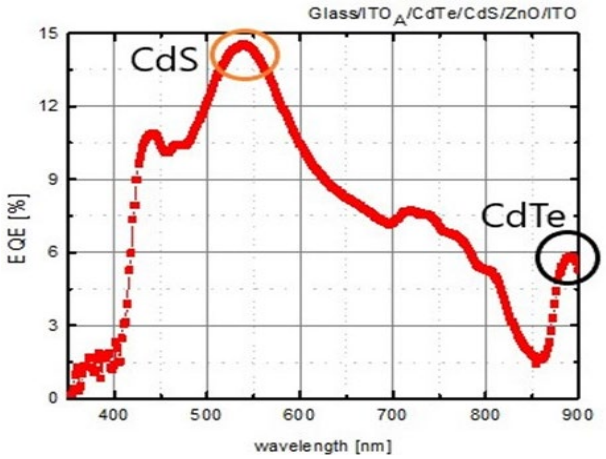

Fig. 7. The action spectrum of the fabricated Glass/ITO$_A$/CdTe/CdS/ZnO/ITO photovoltaic structure.

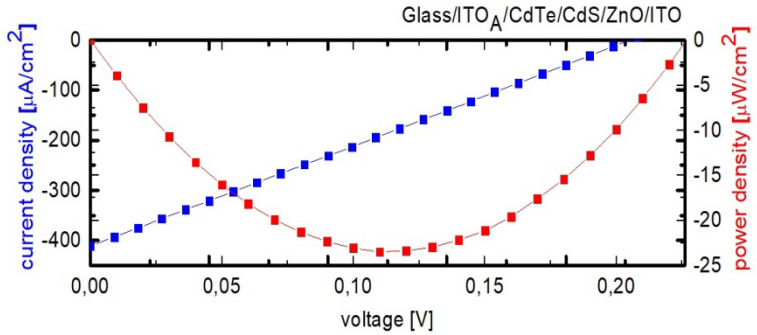

Fig. 8. The current density-voltage (blue line) and power density-voltage (red line) characteristics in AM 1.5 conditions for Glass/ITO$_A$/CdTe/CdS/ZnO/ITO photovoltaic device.

Table 4. Typical parameters in regime of photo-element for Glass/ITO$_A$/CdTe/CdS/ZnO/ITO photovoltaic device.

Sample	V_{oc} (mV)	J_{sc} ($\mu A/cm^2$)	P_{max} (μW)	FF (%)
Glass/ITO$_A$/CdTe/CdS/ZnO/ITO	230	411	23.5	25

In this study, the presented results suggest that the architecture of the electrode assuring the holes transport and their collection play an important role in the photovoltaic performances of fabricated devices. The multi-layered electrode Ag/ZnPc/ZnTe considerably increased the shunt resistance of the samples compared to the ITO electrode, but increased the series resistance too, leading to a decrease of the fill factor. Of course, by optimizing such architectures by using appropriate deposition methods, specific buffer layers, and suitable techniques to improve the

layer interfaces, photovoltaic devices based on ultra-thin films may be a potential alternative to thick CdTe absorber layer samples, but cheaper. On the other hand, in the last time the study of the free Cd A2-B6 thin films are intensively investigated as potential candidates for performant electronic and optoelectronic devices [42-45]

4. Conclusions

Photovoltaic devices, Glass/Ag/ZnPc/ZnTe/CdTe/CdS/ZnO/ITO and Glass/ITO_A/CdTe/CdS/ZnO/ITO, based on ultra-thin film CdTe/CdS heterojunction were fabricated taking into account two architectures of the hole transport and collection back electrode, namely Ag/ZnPc/ZnTe and ITO, conserving the ZnO/ITO configuration as the electron and transport top electrode. The diode factor (n), the reverse saturation current (I_0), and the series (R_s) and shunt (R_{sh}) resistances were evaluated using the modified Shockley-Read equation. The n and I_0 parameters were highly accurate determined by removing sequentially the effects induced by R_s and R_{sh} resistances. It was shown that a hole's transport layer customized as the Ag/ZnPc/ZnTe configuration assures an increased value of R_{sh} but, at the same time, contributes to the increase of the R_s, and, due to this, to the lowering of the photo-electrical parameters, mainly the fill factor. On the other hand, the use of individual ITO layer as back contact, directly on the CdTe absorber film, creates the ITO/CdTe interface which determines a very low R_{sh} and decreases the photo-electrical parameters too, but this time the open circuit photo-voltage is strongly affected.

The specific parameters in the regime of photo-element, such as fill factor (FF), open circuit photo-voltage (V_{oc}), short-circuit current density (J_{sc}), and maximum output power (P_{max}) were computed and analyzed, for an active area of 0.40 cm^2 . The photo-electrical results showed that by combining the advantages given by a multi-layered holes transport structure with the effort to reduce the series resistance by using a ZnO/ITO configuration as an electron transport layer, the overall performances may be increased and such devices can be alternative to thick CdTe absorber based photovoltaic cells but fabricated with lower costs. Anyhow, the optimization process is still young and further studies are required.

Acknowledgments

Research and Development Centre for Materials and Electronic and Optoelectronic Devices of University of Bucharest are acknowledged for instrumental as well as technical support provided.

References

[1] Wu, X.; Dhere, D.S.; Albin, D.S.; Gessert, T.A; Dehart, C.; Keane, J.C.; Duda, A.; Coutts, T.J.; Asher, S.; Levi, D.H.; Moutinho, H.R.; Yan, Y.; Moriarty, T.; Johnston, S.; Emery, K.; Sheldon, P., Proceedings of NCPV Program Review Meeting, Lakewood, USA, 14-17 October 2001.

[2] Green, M.A.; Dunlop, E.D.; Hohl-Ebinger, J.; Yoshita, M.; Kopidakis, N.; Hao, X., Prog Photovolt: Res Appl 28, 629 (2020); https://doi.org/10.1002/pip.3303

[3] Batzner, D.L.; Romeo, A.; Dobeli, M.; Weinert, K.; Zogg, H.; Tiwari, A.N., Conference record of the twenty-ninth IEEE photovoltaic specialists conference, 982 (2002).

[4] Antohe, S.; Ghenescu, V.; Iftimie, S.; Radu, A.; Toma, O.; Ion, L., Dig J Nanomater Biostructures 7, 941 (2012).

[5] Antohe, S.; Iftimie, S.; Ghenescu, V.; Constantineanu, R.; Gugiu, M.M.; Ion, M.; Stan, I.; Radu, A.; Ion, L., Rom Rep Phys 64, 1153 (2012).

[6] Shaaban, E.R.; Osman, M.A.; Osman, A.A.; Sayed, M.M.; Aly, K.I., J Mater Sci Mater

Electron 33, 4051 (2022); https://doi.org/10.1007/s10854-021-07598-4
[7] Toma, O.; Ion, L.; Iftimie, S.; Radu, A.; Antohe, S., Mater Des 100, 198 (2016); https://doi.org/10.1016/j.matdes.2016.03.117
[8] Panaitescu, A.M.; Antohe, I.; Locovei, C.; Iftimie, S.; Antohe, S.; Piraux, L.; Suchea, M.P.; Antohe, V.A., Appl Sci 12, 7808 (2022); https://doi.org/10.3390/app12157808
[9] Ruxandra, V; Antohe, S., J. Appl. Phys. 84 (2), 727-733, (1998); https://doi.org/10.1063/1.368129
[10] Antohe, S.; Ion, L.; Antohe, V. A., Journal of Optoelectronics and Advanced Materials **5**(4), 801 (2003).
[11] Lakmal, A.A.I.; Kumarasinghe, R.K.K.G.R.G.; Seneviratne, V.A.; Thanihaichelvan, M.; Dassanayake, B.S., J Mater Sci Mater Electron 33, 15627 (2022); https://doi.org/10.1007/s10854-022-08467-4
[12] Kumarasinghe, P.K.K.; Dissanayake, A.; Pemasiri, B.M.; Dassanayake, B.S., Mater Res Bull 96, 188 (2017); https://doi.org/10.1016/j.materresbull.2017.04.026
[13] Sebak, M.A.; Ghalab, S.; El-Taher, A.; Shaaban, E.R., Chalcogenide Lett 19, 389 (2022); https://doi.org/10.15251/CL.2022.196.389
[14] Valentovic, D.; Cervenak, J.; Luby, S.; Aldea, M.L.; Botila, T., Phys Status Solidi A 56, 341 (1979); https://doi.org/10.1002/pssa.2210560138
[15] Gupta, A.; Compaan, A.D., Appl Phys Lett 85, 684 (2004); https://doi.org/10.1063/1.1775289
[16] Shao, M.; Ficher, A.; Grecu, D.; Jayamaha, U.; Bykov, E.; Contreras-Puente, G.; Bohn, R.G.; Compaan, A.D., Appl Phys Lett 69, 3045 (1996); https://doi.org/10.1063/1.116834
[17] Bonnet, D., Thin Solid Films 361-362, 547 (2000); https://doi.org/10.1016/S0040-6090(99)00831-7
[18] Chu, T.L.; Chu, S.S.; Ferekides, C.; Wu, C.Q.; Britt, J.; Wnag, C., J Appl Phys 70, 7608 (1991); https://doi.org/10.1063/1.349717
[19] Nor, A.A.-M.; Salim, H.I.; Madugu, M.L.; Olusola, O.I.; Dharmadasa, I.M., Energies 8, 10883 (2015); https://doi.org/10.3390/en81010883
[20] Das, S.K.; Morris, G.C., Sol Energy Mater Sol Cells 28, 305 (1993); https://doi.org/10.1016/0927-0248(93)90118-M
[21] Sivananthan, S.; Chu, X.; Reno, J.; Faurie, J.P., J Appl Phys 60, 1359 (1986); https://doi.org/10.1063/1.337310
[22] Vamsi Krishna, K.; Dutta, V., J Appl Phys 96, 3962 (2004); https://doi.org/10.1063/1.1779952
[23] Moon, B.-S.; Lee, J.-H.; Jung, H., Thin Solid Films 511-512, 299 (2006); https://doi.org/10.1016/j.tsf.2005.11.080
[24] Compaan, A.D.; Gupta, A.; Lee, S.; Wang, S.; Drayton, J., Sol Energy 77, 815 (2004); https://doi.org/10.1016/j.solener.2004.06.013
[25] Panaitescu, A.-M.; Antohe, I.; Raduta, A.-M.; Iftimie, S.; Antohe, S.; Mihailescu, C.N.; Antohe, V.A., AIP Adv 12, 115013 (2022); https://doi.org/10.1063/5.0116999
[26] Panaitescu, A.-M.; Antohe, V.A., Coatings 13, 208 (2023); https://doi.org/10.3390/coatings13010208
[27] Ion, L.; Enculescu, I.; Iftimie, S.; Ghenescu, V.; Tazlaoanu, C.; Besleaga, C.; Mitran, T.L.; Antohe, V.A.; Gugiu, M.M.; Antohe, S., Chalcogenide Lett 7, 521 (2010).
[28] Suthar, D.; Chuhadiya, S.; Sharma, R.; Himanshu; Dhaka, M.S., Mater Adv 3, 8081 (2022); https://doi.org/10.1039/D2MA00817C
[29] Hori, T.; Moritou, H.; Fukuoka, N.; Sakamoto, J.; Fujii, A.; Ozaki, M. Materials 3, 4915 (2010); https://doi.org/10.3390/ma3114915
[30] Michaelson, H.B., J Appl Phys 48, 4729 (1977); https://doi.org/10.1063/1.323539
[31] Whittles, T.J.; Veal, T.D.; Savory, C.N.; Welch, A.W.; de Souza Lucas, F.W.; Gibbon, J.T.; Birkett, M.; Potter, R.J.; Scanlon, D.O.; Zakutayev, A.; Dhanak, V.R., ACS Appl Mater Interfaces 9, 41916 (2017); https://doi.org/10.1021/acsami.7b14208

[32] Oladeji, I.O.; Chow, L.; Ferekides, C.S.; Viswanathan, V.; Zhao, Z., Sol Energy Mater Sol Cells 61, 203 (2000); https://doi.org/10.1016/S0927-0248(99)00114-2

[33] Shalaan, E.; Ibrahim, E.; Al-Marzouki, F.; Al-Dossari, M., Appl Phys A 126, 852 (2020); https://doi.org/10.1007/s00339-020-04045-9

[34] Zhao, S.; Wang, D.X., Opt Quantum Electron 49, 261 (2017); https://doi.org/10.1007/s11082-017-1095-3

[35] Radu, A.; Locovei, C.; Antohe, V.A.; Socol, M.; Coman, D.; Manica, M.; Dumitru, A.; Dan, L.; Radu, C.; Raduta, A.M.; Ion, L.; Iftimie, S.; Antohe, S., Dig J Nanomater Biostructures 15, 679 (2020).

[36] Suthar, D.; Himanshu; Patel, S.L.; Chander, S.; Kannan, M.D.; Dhaka, M.S., J Mater Sci Mater Electron 32, 19070 (2021); https://doi.org/10.1007/s10854-021-06424-1

[37] Munshi, A.H.; Kephart, J.M.; Abbas, A.; Shimpi, T.M.; Barth, K.L.; Walls, J.M.; Sampath, W.S., Sol Energy Mater Sol 176, 9 (2018); https://doi.org/10.1016/j.solmat.2017.11.031

[38] Gorji, N.E.; Reggiani, U.; Sandrolini, L., Sol Energy 118, 611 (2015); https://doi.org/10.1016/j.solener.2015.05.041

[39] Toma O.; Pascu R.; Dinescu M.; Besleaga, C ; Mitran, TL ; Scarisoreanu, N ; Antohe, S ., Chalcogenide Letters, 8(9), 541-548, (2011)

[40] Iftimie, S.; Tazlaoanu, C.; Radu, A.; Constantinescu, R.; Vancea, C.; Korganci, N.; Ion, L.; Antohe, S., Dig J Nanomater Biostructures 9, 213 (2014).

[41] Radu M.; Ghenescu V.; Stan I.; Ion, L ; Besleaga, C; Nicolaev, A ; Mitran, TL ; Tazlaoanu, C ; Radu, A ; Porumb, O; Ghenescu, M ; Gugiu, MM ; Antohe, S., Chalcogenide Letters 8(8), 477-485, (2011)

[42] Toma, O.; Antohe, S., Chalcogenide Letters , 11(11), 611-618, (2014)

[43] Iftimie, S.; Baiasu, F. F.; Radu, A.; Antohe, VA ; Antohe, S ; Ion, L, Chalcogenide Letters 15(7) ,389-394, (2018)

[44] Toma,O.; Ion, L.; Iftimie, S.; Antohe, V.A.; Radu, A.; Raduta, A.M.; Manica, D.; Antohe S., Applied Surface Science, 478,(1) 831-839 (2019); https://doi.org/10.1016/j.apsusc.2019.02.032

[45] Panaitescu, AM and Antohe, VA, Coatings 13(1), (2023) 208; https://doi.org/10.3390/coatings13010208